Convex economic model predictive control for blade loads mitigation on wind turbines

Pamososuryo, Atindriyo Kusumo; Liu, Yichao; Gybel Hovgaard, Tobias; Ferrari, Riccardo; van Wingerden, Jan Willem

DOI
10.1002/we.2869

Publication date
2023

Document Version
Final published version

Published in
Wind Energy

Citation (APA)
Pamososuryo, A. K., Liu, Y., Gybel Hovgaard, T., Ferrari, R., & van Wingerden, J. W. (2023). Convex economic model predictive control for blade loads mitigation on wind turbines. *Wind Energy*, *26*(12), 1276-1298. https://doi.org/10.1002/we.2869

Important note
To cite this publication, please use the final published version (if applicable).
Please check the document version above.

Received: 3 February 2023 | Revised: 5 April 2023 | Accepted: 29 August 2023

DOI: 10.1002/we.2869

RESEARCH ARTICLE

WILEY

Convex economic model predictive control for blade loads mitigation on wind turbines

Atindriyo Kusumo Pamososuryo[1] | Yichao Liu[1] | Tobias Gybel Hovgaard[2] | Riccardo Ferrari[1] | Jan-Willem van Wingerden[1]

[1]Delft Center for Systems and Control, Faculty of Mechanical, Maritime, and Materials Engineering, Delft University of Technology, Delft, The Netherlands

[2]Vestas Technology R&D, Vestas A/S, Aarhus, Denmark

Correspondence
Atindriyo Kusumo Pamososuryo, Delft Center for Systems and Control, Faculty of Mechanical, Maritime, and Materials Engineering, Delft University of Technology, Mekelweg 2, 2628 CD, Delft, The Netherlands.
Email: A.K.Pamososuryo@tudelft.nl

Present address
Atindriyo Kusumo Pamososuryo, Delft Center for Systems and Control, Faculty of Mechanical, Maritime, and Materials Engineering, Delft University of Technology, Mekelweg 2, 2628 CD, Delft, The Netherlands.

Abstract

Economic model predictive control (EMPC) has received increasing attention in the wind energy community due to its ability to trade-off economic objectives with ease. However, for wind turbine applications, inherent nonlinearities, such as from aerodynamics, pose difficulties in attaining a convex optimal control problem (OCP), by which real-time deployment is not only possible but also a globally optimal solution is guaranteed. A variable transformation can be utilized to obtain a convex OCP, where nominal variables, such as rotational speed, pitch angle, and torque, are exchanged with an alternative set in terms of power and energy. The ensuing convex EMPC (CEMPC) possesses linear dynamics, convex constraints, and concave economic objectives and has been successfully employed to address power control and tower fatigue alleviation. This work focuses on extending the blade loads mitigation aspect of the CEMPC framework by exploiting its individual pitch control (IPC) capabilities, resulting in a novel CEMPC-IPC technique. This extension is made possible by reformulating static blade and rotor moments in terms of individual blade aerodynamic powers and rotational kinetic energy of the drivetrain. The effectiveness of the proposed method is showcased in a mid-fidelity wind turbine simulation environment in various wind cases, in which comparisons with a basic CEMPC without load mitigation capability and a baseline IPC are made.

KEYWORDS
blade loads mitigation, convex economic model predictive control, economic objectives trade-off, individual pitch control

1 | INTRODUCTION

Horizontal axis wind turbine rotor sizes have been consistently increased to improve nameplate power ratings.[1] However, being ever longer and more flexible, wind turbine blades experience exacerbated asymmetric loadings due to the greater influence of turbulence, wind shear, tower shadow, and yaw misalignment.[2] Such wind spatiotemporal variability gives rise to the spectral contents of the blade loads at once-per-rotation (1P) frequency and its higher harmonics (2P, 3P, etc.), which are reflected as 0P, 3P, 6P, and so on at the fixed support structure for three-bladed turbines.[3] These fatigue loadings, accumulated over time, may eventually lead to irreversible damage—impeding economic benefits of power

generation from being attained as wind turbine lifetime becomes shorter. Hence, the importance of advanced control strategies with the capabilities to handle fatigue load minimization alongside power production maximization becomes higher than ever.

Individual pitch control (IPC), by which wind turbine blades are individually actuated in response to measured out-of-plane (OoP) blade root bending moments, has played a pivotal role in alleviating the aforementioned asymmetric loads. In conventional IPC, these blade load signals in the rotating frame, containing dominant 1P frequency, are projected by an azimuth-dependent Coleman transformation[3] onto tilt and yaw axes in the fixed frame. On these orthogonal axes, a pair of identical single-input single-output (SISO) controllers, such as proportional-integral (PI) compensators[2] or simple integrators,[4] is then designed for canceling the static (0P) tilt and yaw loads to create blade pitch commands on each axis. A reverse Coleman transformation subsequently projects the blade pitch signals back into the rotating frame to obtain 1P individual pitch actions, thus reducing the 1P and 0P load components in the respective rotating and fixed parts of the turbine.[2,4]

Aside from PI and other loop-shaping methods alike, different approaches to realize blade loads mitigation are also present in the literature. Optimal state-feedback methods, such as linear quadratic regulator[5] and linear quadratic Gaussian,[2,6,7] were considered, in which state regulation and control input penalization trade-off tuning are accommodated. Others investigated H_∞-based approaches,[8–10] which are capable of handling multivariable systems as well as accounting for uncertainties in the model and measurements. In spite of their advantages, these classes of controllers are not able to altogether (1) take into account system constraints, (2) address multivariable systems with ease, (3) provide convenient trade-offs between different control objectives, and (4) predict the future behavior of the system given current (or preview) information, several properties of which are inherent in model predictive control (MPC) designs.[11]

MPC is a model-based control algorithm that optimizes a system's inputs to attain certain control objectives over a finite prediction horizon in the future while adhering to the system's constraints.[12] In the vast majority of MPC implementations, tracking objectives are employed within its optimization control problem (OCP) formulation to steer a system to certain precalculated steady-state references, known as the tracking MPC (TMPC). Several studies have demonstrated the potential of TMPC for wind turbine applications, such as for power control, tower damping, blade loads mitigation, and combinations thereof.[13–18] Regardless of the demonstrated good performance, TMPC is somewhat lacking in terms of the straightforward connection between its tracking objective and the actual objective of wind turbine operation, namely, economic performance.[19] On top of that, a common assumption that tracking steady-state references bring the most profit may not necessarily be true, particularly during transients.[20] Fortunately, these predicaments can be tackled by the incorporation of economic objectives in place of reference tracking ones, resulting in the economic MPC (EMPC).

Early work on EMPC for wind turbine control focused on the power maximization aspect and development of 'turnpike'* correction, which has hindered short time horizon implementation of EMPC,[19] with an extension followed, in which tower fatigue mitigation and trade-off tuning by Pareto front are accounted for.[21] In these works, quasi-convex OCPs are employed, where the convexity of the formulated OCPs holds in a certain operating region. A number of studies incorporating convex EMPC (CEMPC) methods, by which a globally optimal solution is ensured and real-time implementation is made possible, have been investigated. As an instance, CEMPC has been employed for preventing soft-soft tower resonance in the presence of rotor imbalance at the below-rated region by frequency-skipping.[22] The convexity of the OCP in this framework owes to the property of the wind turbine dynamics incorporated therein, cast as that of quasi-linear parameter-varying by a model demodulation transformation technique. Another OCP convexification strategy in the literature is realized by transforming nominal wind turbine variables into power and energy terms such as rotational kinetic energy, aerodynamic power, and generator power to obtain concave objectives (to be maximized), linear dynamics, and convex constraints. The optimal control inputs resulting from the optimization routine then undergo a reverse variable transformation to obtain implementable wind turbine signals in the nominal variables, such as blade pitch and generator torque demands. Such a CEMPC concept was initially introduced with the goal of ensuring the smoothness of grid power delivery with an integrated local storage system.[23]

Some research efforts followed afterward, extending the latter CEMPC framework to account for fore-aft[24,25] and side-side[26] tower fatigue loads mitigation. Of particular interest is the latter extension since an individual pitching strategy was favored over the more conventional approach by generator torque control in order to lessen the variation of the generated power as a by-product of the damping activities. The decomposition of a single aerodynamic power acting on the rotor into multiple components, referring to those of the blades, has become a key to realizing individual pitching within the framework. By reformulation of the side-side blade forces in terms of these aerodynamic powers and rotational kinetic energy, a tower-top force counteracting tower vibrations can be created by CEMPC. Yet, little to no attention is paid to the augmentation of a blade loads mitigation objective, exploiting further the IPC potential of the CEMPC framework.

This paper thus aimed to fill the knowledge gap by incorporating an individual pitching mechanism for blade loads alleviation into the CEMPC framework by the authors.[23,26] In detail, this extension includes OoP blade root bending moments and rotor tilt and yaw moments as parts of the wind turbine model description. By recasting these moments, alongside simplified drivetrain dynamics and relevant constraints, into their equivalence in terms of individual aerodynamic powers and rotational kinetic energy, linear dynamics and convex constraints are obtained. On top of that, employing concave objective functions (to be maximized) results in a convex OCP, by which not only globally optimal control inputs (with respect to the internal model and available information through measurement and estimation data) are guaranteed but also real-time implementation is made possible. Furthermore, the benefit of EMPC, in terms of convenient trade-off tuning capability between different economic

*In this case, it is the total absorption of rotor kinetic energy for power generation, resulting in an entirely stopped rotor.

objectives, can also be performed. For the remaining parts of this paper, this novel method is referred to as the "CEMPC-IPC." The contributions of this work are now in order as follows:

1. Establishing linear wind turbine dynamics and convex constraints suitable for blade loads mitigation by individual pitching by application of a variable transformation in power and energy terms to a nominal wind turbine model description;
2. Formalizing a convex OCP by incorporation of concave economic objective functions (to be maximized), which cater for the penalization of rotor tilt and yaw moments, on top of the linear dynamics and convex constraints;
3. Integrating the Coleman blade-effective wind speed estimator,[27] as well as an unscented Kalman filter for rotor tilt and yaw moment biases estimation, to supply the proposed CEMPC-IPC with unknown and unmeasurable quantities;
4. Showcasing the performance of the CEMPC-IPC in a mid-fidelity wind turbine simulation environment under artificial and realistic wind profiles, including comparisons with a basic CEMPC and a conventional IPC.

The remainder of this paper proceeds as follows. Section 2 describes a nonlinear reduced-order wind turbine dynamical model along with their constraints in the nominal wind turbine variables. Section 3 elaborates on the derivation of the linear wind turbine dynamics and convex constraints by a transformation of variables in power and energy terms. The formulation of the convex economic OCP of the proposed CEMPC-IPC is laid out in Section 4, where the required estimator designs are also discussed. In Section 5, the effectiveness of the CEMPC-IPC is demonstrated in a mid-fidelity computer-aided wind turbine simulation setup FAST (Fatigue, Aerodynamics, Structures, and Turbulence)[28] by the National Renewable Energy Laboratory (NREL). Finally, in Section 6, the concluding remarks of this work are given.

2 | WIND TURBINE MODEL

In model-based control methods such as MPC, obtaining a system's dynamic model is a critical first design step. To prevent a too high computational burden, a reduced-order model with the ability to capture the most relevant dynamics according to the control objectives is preferable over high-order ones. In this section, the first-principles derivation of the nominal wind turbine model comprising of drivetrain dynamics and static blade and rotor moments is conducted in Sections 2.1 and 2.2, respectively. In Section 2.3, several remarks regarding potential nonconvexity ensuing from model nonlinearities, motivating the adoption of variable transformation in the power and energy terms, are laid out.

2.1 | Drivetrain dynamics

To model a wind turbine drivetrain, a single mass representation of the drivetrain dynamics on the high-speed shaft (HSS) side is considered, which is governed by the following equation[23]

$$J_{\text{hss}}\dot{\omega}_{\text{g}}(t) = T_{\text{r}}(t)/G - T_{\text{g}}(t), \tag{1}$$

with t being the continuous time notation. The HSS equivalent inertia is denoted by $J_{\text{hss}} = J_{\text{g}} + J_{\text{r}}/G^2$, with J_{g}, J_{r}, and $G \geq 1$ as the generator inertia, rotor inertia, and gearbox ratio, respectively. The notation ω_{g} represents the generator rotational speed, being a system's state, operated within the range

$$0 \leq \omega_{\text{g}}(t) \leq \omega_{\text{g,max}}, \tag{2}$$

where $\omega_{\text{g,max}}$ is the maximum allowable speed for the generator, chosen to be 130% of the rated value $\omega_{\text{g,rated}}$. The generator torque T_{g} is a control input constrained by

$$0 \leq T_{\text{g}}(t) \leq T_{\text{g,rated}}, \tag{3}$$

with $T_{\text{g,rated}}$ defined as the rated generator torque producing wind turbine nameplate power rating $P_{\text{g,rated}}$ at $\omega_{\text{g,rated}}$, taking into account the generator efficiency.

The aerodynamic torque T_{r} is often modeled as a single quantity affecting the entire rotor disk, including in the original CEMPC work.[23] Nevertheless, it can also be thought of as the sum of multiple blade-effective quantities[6,26] $T_{\text{r},i}$, with $i \in \{1,2,3\}$ for three-bladed wind turbines, which is especially beneficial for IPC formulations, as considered in this work. This accumulation of individual blade torques is expressed by the following relation:

$$T_r(t) = \sum_{i=1}^{3} T_{r,i}(t). \tag{4}$$

As the blades rotate under the same rotor speed $\omega_r = \omega_g/G$ altogether, their extracted aerodynamic powers from the wind contribute to that of the rotor disk P_r as

$$P_r(t) = \omega_r(t) \sum_{i=1}^{3} T_{r,i}(t) = \sum_{i=1}^{3} P_{r,i}(t), \tag{5}$$

in which

$$P_{r,i}(t) = \frac{1}{6}\rho A C_p(\omega_r(t), \beta_i(t), v_i(t)) v_i(t)^3. \tag{6}$$

The air density, considered to be 1.225 kg/m^3, and the rotor area are denoted, respectively, by ρ and $A = \pi R^2$, with R being the radius of the rotor. The notation C_p refers to the aerodynamic power coefficient, being a function of ω_r, the blade-effective wind speed (BEWS) v_i, and the individual blade pitch β_i, constrained by

$$\beta_{min} \le \beta_i(t) \le \beta_{max}. \tag{7}$$

Such a coefficient is commonly provided in the form of a look-up table, the data of which are collected from simulations at different operating points.

The main output of the drivetrain operation is the generated power, computed as follows:

$$P_g(t) = \eta_g \omega_g(t) T_g(t), \tag{8}$$

with the efficiency factor $\eta_g \in (0, 1]$ accounting for losses due to the mechano-electrical power conversion. The produced power is subjected to the following constraints

$$0 \le P_g(t) \le P_{g,max}(t), \tag{9}$$

with the maximum generated power defined as[24]

$$P_{g,max}(t) = \min\left(\eta_g \omega_g(t) T_{g,rated}, P_{g,rated}\right), \tag{10}$$

which varies based on the current ω_g and holds P_g constant at $P_{g,rated}$ when ω_g excurses above $\omega_{g,rated}$ to prevent generator overloading.

2.2 | Static blade and rotor moments formulation

To incorporate blade loads mitigation aspects into the proposed CEMPC-IPC, additional differential equations may be employed to model the dynamics of the blades[13,29] at the expense of increased model order and thus, computational demand. An alternative path is to employ static blade moments based on the blade-element momentum (BEM) theory,[6,30] such as adopted in this paper.

As briefly mentioned in Section 1, the OoP blade root bending moment $M_{op,i}$ suffers from severe 1P fatigue loading from the spatial and temporal variations in the wind over the rotor disk and hence subject of mitigation by the proposed CEMPC-IPC. As illustrated in Figure 1, such a moment is built by a thrust or normal force $F_{t,i}$ acting on a particular distance from the rotor center

$$M_{op,i}(t) = s_c F_{t,i}(t) R, \tag{11}$$

where the scaling factor $s_c = 2/3$ for a linearly increasing force distribution along the blade span.[6] The individual blade thrust force in the above expression is defined as

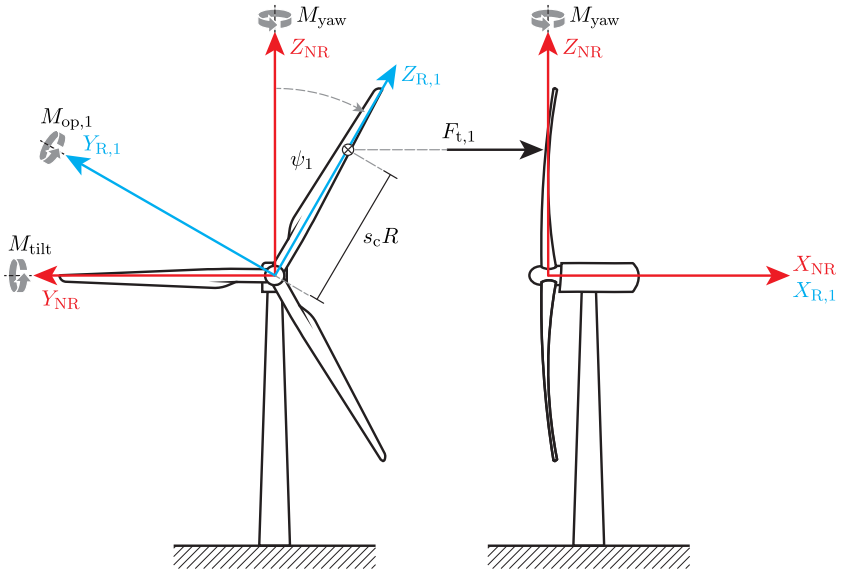

FIGURE 1 First blade thrust force $F_{t,1}$, shown to act at $s_c R$ from the rotor center, with s_c being a scaling factor and R the rotor radius. Subsequently, the out-of-plane blade root bending moment $M_{op,1}$ is created in the rotating reference frame (blue axes). The projections of $M_{op,i}$, $i \in \{1,2,3\}$, in the nonrotating reference frame (red axes), that is, the tilt (M_{tilt}) and yaw moments (M_{yaw}), are obtained by means of the azimuth-dependent forward Coleman transformation, where the first blade azimuth is indicated by ψ_1. Note that the origins of both reference frames are situated at the rotor apex with their X axes directed toward the downwind direction.

$$F_{t,i}(t) = F_{dyn,i}(t) C_t(\omega_r(t), \beta_i(t), v_i(t)), \tag{12}$$

with

$$F_{dyn,i}(t) = \frac{1}{6} \rho A v_i(t)^2, \tag{13}$$

being the dynamic force. The aerodynamic thrust coefficient C_t, similar to C_p, is a function dependent on ω_r, β_i, and v_i.

As depicted in Figure 1, the loads experienced by $M_{op,i}$ are also transferred to the support structure in tilt and yaw (or horizontal and vertical) directions, therefore designing controllers on these axes to mitigate both load components are of interest. This requires the projection $M_{op,i}$ from the rotating frame onto the nonrotating tilt and yaw axes,

$$M_{tilt}(t) = \frac{2}{3} \sum_{i=1}^{3} M_{op,i}(t) \cos(\psi_i(t)), \tag{14}$$

and

$$M_{yaw}(t) = \frac{2}{3} \sum_{i=1}^{3} M_{op,i}(t) \sin(\psi_i(t)), \tag{15}$$

respectively, which is known as the forward Coleman transformation. The azimuth angle of the i-th blade $\psi_i = \int \omega_r dt + 2\pi(i-1)/3$ is considered to be 0° at vertically upward position and increases in the clockwise direction. The original Coleman transformation also involves the computation of the collective component of $M_{op,i}$; however, as this component serves little to no relevance for IPC designs, it is often disregarded.

2.3 | Potential nonconvexity and related challenges for CEMPC-IPC design

Several remarks need to be made regarding the formulated wind turbine model in Sections 2.1 and 2.2, which can also be expressed as the following general state space representation:

$$\begin{cases} \dot{x}(t) = f(x(t), \mathbf{u}(t), \mathbf{d}(t)) \\ \mathbf{y}(t) = g(x(t), \mathbf{u}(t), \mathbf{d}(t)) \end{cases}, \tag{16}$$

with the respective state, inputs, disturbances, and outputs as follows:

$$\begin{cases} x(t) = \omega_g(t) \\ \mathbf{u}(t) = [\beta_1(t), \beta_2(t), \beta_3(t), T_g(t)]^\top \\ \mathbf{d}(t) = [v_1(t), v_2(t), v_3(t)]^\top \\ \mathbf{y}(t) = [\omega_g(t), P_g(t), M_{\text{tilt}}(t), M_{\text{yaw}}(t)]^\top \end{cases}. \tag{17}$$

In particular, the nonlinearities contained in (16) in the variables (17) may result in nonconvexity during the economic model predictive controller design phase. These nonlinearities are highlighted hereunder:

1. The coefficient C_p is a nonlinear function in the above-mentioned variables, particularly ω_g, β_i, and v_i, which, combined with the cube of the wind speed v_i^3, renders $P_{r,i}$ also nonlinear in these variables. As $T_{r,i}$ carries over such nonlinearities through the relation (5), the drivetrain dynamics (1) or, similarly, $\dot{x}$ in (16), are thus nonlinear in nature;
2. The generated power P_g is bilinear in ω_g and T_g as shown in (8), which is another form of nonlinearity contained in the model, in particular in the output vector $\mathbf{y}$;
3. Similar to C_p, the coefficient C_t contained in $F_{t,i}$ is nonlinear in ω_g, β_i, and v_i. Together with the squared wind speed v_i^2, $F_{t,i}$ becomes nonlinear in the variables (17). This is carried over to $M_{op,i}$ as expressed in (11) and subsequently to $\mathbf{y}$ by M_{tilt} and M_{yaw} as shown in relations (14) and (15).

The above existing nonlinearities may ensue in a nonconvex OCP formulation of EMPC. Such an OCP promotes the utilization of nonconvex programming methodologies, in which a globally optimal solution is not guaranteed to be found, not to mention the resulting higher computational complexities. A possible solution to this challenge is by applying first-order Taylor expansion to the nonlinear quantities so as to obtain their Jacobian matrices, which are linear in their variables. One may also opt for variable transformation capable of rendering the dynamics and constraints suitable for convex optimization algorithms.[23,26] The latter approach is adopted in this study and discussed in the next section.

3 | TRANSFORMED WIND TURBINE MODEL

Being nonlinear in its variables, the wind turbine model derived in Section 2 needs to be recast into an alternative one suitable for CEMPC-IPC deployment. The main idea is to substitute a number of variables in (17), specifically ω_g, β_i, and T_g with rotational kinetic energy K_g, $P_{r,i}$, and P_g, respectively, which results in the following new set of variables

$$\begin{cases} x_t(t) = K_g(t) \\ \mathbf{u}_t(t) = [P_{r,1}(t), P_{r,2}(t), P_{r,3}(t), P_g(t)]^\top \\ \mathbf{d}_t(t) = [v_1(t), v_2(t), v_3(t)]^\top \\ \mathbf{y}_t(t) = [K_g(t), P_g(t), M_{\text{tilt}}(t), M_{\text{yaw}}(t)]^\top \end{cases}. \tag{18}$$

Accordingly, the change of the system's state from x to x_t above necessitates the drivetrain dynamics (1) and the corresponding system constraints, namely (2), (3), (7), and (9), to be re-expressed in the new terms. Since such a dynamics reformulation has been treated in the previous CEMPC works,[23,26] only brief summary of its derivation is presented in Section 3.1. Moreover, despite being kept as outputs in (18), the rotor moments M_{tilt} and M_{yaw} are still functions of the nominal variables (17) such that their equivalence in power and energy variables is yet to be established. This reformulation constitutes one of the main contributions of this study and is treated in Section 3.2.

3.1 | Kinetic energy dynamics

Following the introduction of the new variables (18), the drivetrain dynamics previously described as a torque balance equation are now rewritten as the rate-of-change (ROC) of the stored rotational kinetic energy $K_g = (J_{hss}/2)\omega_g^2$, namely,

$$\dot{K}_g(t) = J_{hss}\dot{\omega}_g(t)\omega_g(t) = \left(\sum_{i=1}^{3} T_{r,i}(t)/G - T_g(t)\right)\omega_g(t) = \sum_{i=1}^{3} P_{r,i}(t) - P_g(t)/\eta_g. \tag{19}$$

This expression enables a new perspective to see the drivetrain dynamics as a power balance equation and is linear in their inputs. It is thus subject to the bounds on K_g, which are readily obtained by calculating the kinetic energies of $\omega_{g,min}$ and $\omega_{g,max}$ in (2)

$$(J_{hss}/2)\omega_{g,min}^2 \le K_g(t) \le (J_{hss}/2)\omega_{g,max}^2, \tag{20}$$

and to the constraints of the inputs $P_{r,i}$ and P_g explained in the following.

The ability provided by $P_{r,i}$ to store energy in the rotating system (19) is limited by the rotor aerodynamic characteristics embodied in C_p, which is dependent not only on $\omega_r = \sqrt{2K_g/J_{hss}}/G$ and v_i but also on the freedom in the pitching of the blades within the allowed range (7). Such a limit is known as the "available wind power," which is formulated below

$$P_{av,i}(K_g(t), v_i(t)) = \max_{\beta_{min} \le \beta_i(t) \le \beta_{max}} \frac{1}{6}\rho A C_p\left(\sqrt{2K_g(t)/J_{hss}}/G, \beta_i(t), v_i(t)\right) v_i(t)^3. \tag{21}$$

The above expression is still nonconcave of K_g, which motivates its concave approximation, in the form of piecewise linear (PWL) functions, to be formulated[23] as follows:

$$\check{P}_{av,i}(K_g(t), v_i(t)) = \min\{a_1 K_g(t) + b_1, \ldots, a_j K_g(t) + b_j\} v_i(t)^3, \tag{22}$$

where a_m and b_m, with $m \in \{1,\ldots,j\}$, are the PWL functions' coefficients. Therefore, the constraints for $P_{r,i}$ are formalized as follows:

$$0 \le P_{r,i}(t) \le \check{P}_{av,i}(K_g(t), v_i(t)), \tag{23}$$

which is concave in K_g. The reader interested in the detailed derivation of the above constraints is referred to the work of Hovgaard et al.[23]

Remark 1. A note must be taken that in (21), β_{min} is considered the minimum pitch angle before reaching the stall region. As this minimum angle differs for different combinations of K_g and v_i, the coefficient table C_p is preprocessed accordingly before reformulated into $P_{av,i}$.

As for P_g, its bounds in (9) can be rewritten in terms of K_g as follows:[24.]

$$0 \le P_g(t) \le \min\left(\eta_g\sqrt{2K_g(t)/J_{hss}}T_{g,rated}, P_{g,rated}\right), \tag{24}$$

which are convex in P_g and concave in K_g. It is important to note the use of P_g directly as a variable is advantageous in that linearization of (9) about $P_{g,rated}$ (due to the bilinearity in ω_g and T_g as pointed out in Section 2.3) is precluded. Such linearization introduces a certain degree of conservativeness since $P_{g,rated}$ may not always be reached when ω_g deviates too far from the linearization point.[31]

3.2 | Static blade and rotor moments in power and energy terms

In a previous work,[26] individual pitching for mitigating side-side tower excitation within the same CEMPC framework was developed. Therein, the inclusion of IPC into the framework is made possible by virtue of lateral blade force transformation to power and energy variables. In the current paper, a similar idea of enabling IPC for blade loads reduction is adopted in the framework. It is realized by rewriting $F_{t,i}$ in the new variables, followed by its substitutions into the blade moment $M_{op,i}$ and, afterward, rotor moments M_{tilt} and M_{yaw}.

To this end, the following relation between power and torque coefficients $C_p = \lambda_i C_q$ is considered, with $\lambda_i = \sqrt{2K_g/J_{hss}}R/Gv_i$ being the tip-speed ratio expressed in the new variables. The individual aerodynamic power Equation (6) now becomes

$$P_{r,i}(t) = \underbrace{\frac{1}{6}\rho A v_i(t)^2}_{F_{dyn,i}(t)}\left(\sqrt{2K_g(t)/J_{hss}}/G\right) R C_q\left(\sqrt{2K_g(t)/J_{hss}}/G, \beta_i(t), v_i(t)\right),$$

which contains $F_{\text{dyn},i}$ from (13) as indicated. The above realization paves the way for $F_{\text{dyn},i}$ to be rewritten in terms of power and energy as follows:

$$F_{\text{dyn},i}(t) = \frac{P_{\text{r},i}(t)}{\left(\sqrt{2K_{\text{g}}(t)/J_{\text{hss}}}/G\right)R} \frac{1}{C_{\text{q}}\left(\sqrt{2K_{\text{g}}(t)/J_{\text{hss}}}/G, \beta_i(t), v_i(t)\right)}.$$

By application of the above definition of $F_{\text{dyn},i}$ into (12), the individual blade thrust force can be readily recast into

$$F_{\text{t},i}(t) = \frac{P_{\text{r},i}(t)}{\left(\sqrt{2K_{\text{g}}(t)/J_{\text{hss}}}/G\right)R} C_{\text{t/q}}\left(\sqrt{2K_{\text{g}}(t)/J_{\text{hss}}}/G, \beta_i(t), v_i(t)\right), \tag{25}$$

with $C_{\text{t/q}}$ as the shorthand notation for $C_{\text{t}}/C_{\text{q}}$. Note that the inverse square root of the kinetic energy $1/\sqrt{K_{\text{g}}}$ contained in (25) is nonconvex in K_{g}. In addition, the coefficient $C_{\text{t/q}}$ is nonlinear in the variables K_{g}, β_i, and v_i, with β_i being one of the nominal variables. To tackle these additional complexities in rendering $F_{\text{t},i}$ convex in its variables, several assumptions are thus needed.

Assumption 1. It is assumed that K_{g} varies slowly over time, such that in the implementation of CEMPC-IPC later on in Section 4, it can be considered constant based on the current turbine measurements for the computations of $F_{\text{t},i}$.

Assumption 2. The calculation of $C_{\text{t/q}}$ takes constant K_{g} as indicated in Assumption 1, β_i of the previous CEMPC-IPC solution, and constant v_i based on the current wind speed information. This effectively leaves $P_{\text{r},i}$ as the only decision variable for determining $F_{\text{t},i}$.

The ensuing OoP blade root bending moment in power and energy terms is obtained straightforwardly by substitution of (25) into (11) that results in

$$M_{\text{op},i}(P_{\text{r},i}(t)) = s_{\text{c}} \frac{P_{\text{r},i}(t)}{\left(\sqrt{2\tilde{K}_{\text{g}}(t)/J_{\text{hss}}}/G\right)} C_{\text{t/q}}\left(\sqrt{2\tilde{K}_{\text{g}}(t)/J_{\text{hss}}}/G, \tilde{\beta}_i(t), \tilde{v}_i(t)\right)R, \tag{26}$$

where the quantities in which Assumptions 1 and 2 hold are indicated by tilde $(\tilde{\cdot})$ notations. The following and the last step in the static blade forces and moments derivation in power and energy terms is the application of forward Coleman transformation to (26). However, note that the use of trigonometric functions $\cos(\psi_i)$ and $\sin(\psi_i)$, with $\psi_i = \int\left(\sqrt{2K_{\text{g}}/J_{\text{hss}}}/G\right)\text{d}t + 2\pi(i-1)/3$, in (14) and (15) indicates additional nonconvexities in K_{g}, for which the following additional assumption is required.

Assumption 3. The azimuth ψ_i is taken from the measurements, which is also forward-propagated for the entire prediction horizon of the CEMPC-IPC given the measurements of ω_{r}.

Taking Assumption 3 into account, rotor tilt and yaw moments previously defined in (14) and (15) are now rewritten as

$$M_{\text{tilt}}(t) = \frac{2}{3}\sum_{i=1}^{3} M_{\text{op},i}(P_{\text{r},i}(t))\cos(\tilde{\psi}_i(t)), \tag{27}$$

and

$$M_{\text{yaw}}(t) = \frac{2}{3}\sum_{i=1}^{3} M_{\text{op},i}(P_{\text{r},i}(t))\sin(\tilde{\psi}_i(t)), \tag{28}$$

with $\tilde{\psi}$ denoting the measured/forward-propagated azimuth position.

4 | CONVEX ECONOMIC MODEL PREDICTIVE CONTROL SETUP

An OCP is at the heart of every model predictive controller design, including the CEMPC-IPC proposed in this work. Comprising the system dynamics, constraints, and objective functions, it is solved to optimize the prediction of a system's behavior up to a finite time horizon in the

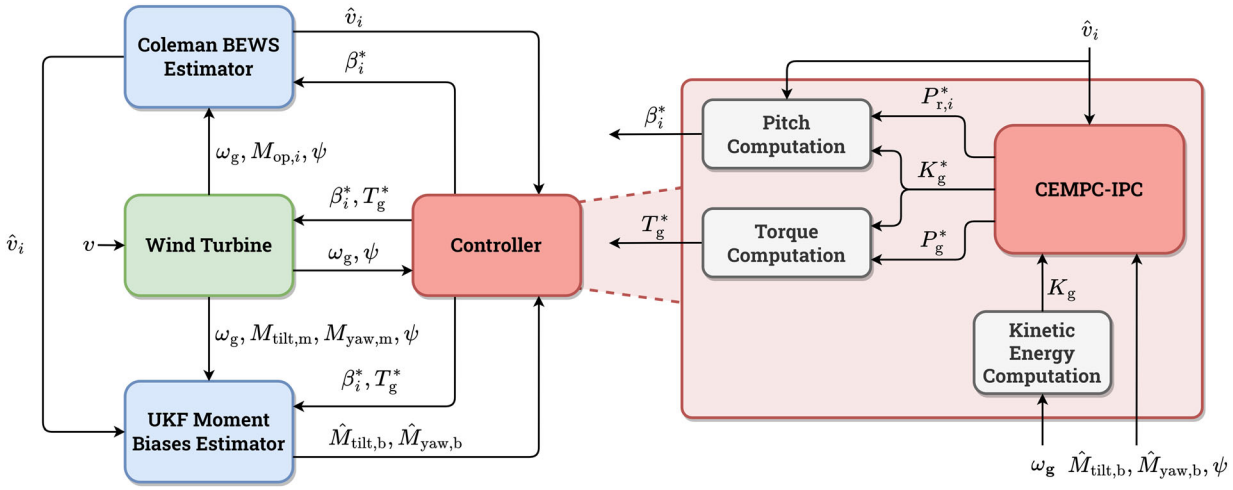

FIGURE 2 Convex EMPC (CEMPC)-individual pitch control (IPC) implementation setup. A blade-effective wind speed (BEWS) and moment biases estimator via unscented Kalman filtering (UKF) are included for providing unknown information to the controller.

future. The product of such optimization is an optimal input trajectory, the first element of which is applied to the system. The measured response due to the application of the optimal input is thus taken by CEMPC-IPC to restart the optimization so as to produce the subsequent optimal input trajectory with a one-step-ahead roll in the horizon.

In Section 4.1, the OCP formulation for the proposed CEMPC-IPC is discussed, in which several economic objective functions are presented and incorporated with the transformed wind turbine dynamics and constraints derived previously in Section 3. Moreover, as not all quantities needed to begin the optimization routine are available from the measurements, state estimators need to be integrated, which are explained in Section 4.2. Figure 2 illustrates the diagram showing the interconnection of these subsystems.

4.1 | Optimal control problem formulation

As a subclass of EMPC, CEMPC inherits its feature in the sense that a system's economic performance, manifested in concave objective functions, is maximized instead of targeting the system to reach steady-state references, as done in TMPC. In the previous works,[23,26] power production maximization, reduction of overspeeding duration, and minimization of excessive actuation aspects of the wind turbine economic performance have been addressed, which are also taken into consideration here. Moreover, as an extension of these works, this study now accounts for the blade loads alleviation aspect, thereby extending the structural loads mitigation capability of the framework. Thus, for the purpose of realizing CEMPC-IPC, the following economic objective functional concave in the new variables (18) is proposed

$$\mathcal{J}_{\mathrm{OCP}}(t) = w_1 P_{\mathrm{g}}(t) + w_2 \sum_{i=1}^{3} \check{P}_{\mathrm{av},i}(v_i(t), K_{\mathrm{g}}(t)) - w_3 K_{\mathrm{g,slack}}(t)^2 - w_4 \sum_{i=1}^{3} \dot{P}_{\mathrm{r},i}(t)^2 - w_5 \dot{P}_{\mathrm{g}}(t)^2 - w_6 M_{\mathrm{tilt}}(t)^2 - w_7 M_{\mathrm{yaw}}(t)^2, \tag{29}$$

where w_l, $l \in \{1,\ldots,7\}$ is the corresponding weight of each term. The interpretation of each objective is explained below.

The first term of (29) refers to the main objective of the power control, that is, to achieve maximum generated power. To push the upper bound of the operable $P_{\mathrm{r},i}$ (as shown in (22)) higher such that the maximum available power in the wind can be extracted, the second term is included. The third term corresponds to the overspeeding penalization for reducing the duration in which K_{g} excurses from its rated value $K_{\mathrm{g,rated}} = (J_{\mathrm{hss}}/2)\omega_{\mathrm{g,rated}}^2$ by enforcement of the following constraints

$$K_{\mathrm{g}}(t) \le K_{\mathrm{g,rated}} + K_{\mathrm{g,slack}}(t), \text{ with } K_{\mathrm{g,slack}}(t) \ge 0, \tag{30}$$

where $K_{\mathrm{g,slack}}$ is a slack variable, which is realized by collective pitching to prevent $P_{\mathrm{r},i}$ from transferring more power to the drivetrain than the generator is able to cope with. To prevent aggressive actuators activities of β_i and T_{g}, penalties on the ROC of the aerodynamic power $\dot{P}_{\mathrm{r},i}$ and generated power $\dot{P}_{\mathrm{g}}$ are incorporated in the respective fourth and fifth terms. The sixth and seventh terms play a central role in the blade loads mitigation aspect of CEMPC-IPC as these represent the objectives to minimize the asymmetric loadings over the rotor area reflected in M_{tilt} and M_{yaw}.

Having the linear dynamics, convex constraints, and concave objective functions formulated, the convex OCP of the proposed CEMPC-IPC for blade loads mitigation can now be formalized as the following equation

$$\max_{\mathbf{U}_t} \sum_{k=0}^{N_p-1} \mathcal{J}_{\mathrm{OCP}}(k), \tag{31a}$$

$$\text{s.t.} \quad x_t(k+1) = A_d x_t(k) + \mathbf{B}_d \mathbf{u}_t(k), \tag{31b}$$

$$x_t(0) = x_{t,0}, \tag{31c}$$

$$(20),(23),(24),(30), \tag{31d}$$

with k and N_p being the discrete time notation and prediction horizon of the controller. The notations A_d and $\mathbf{B}_d$ in (31b) designate the respective discrete state and input matrices of the transformed wind turbine dynamics (19)—by which the turbine state is predicted, discretized using the Tustin/trapezoidal method[32] under the sampling time T_s. To initialize the prediction, the internal state of the controller $x_t(0)$ is taken from the measurement $x_{t,0}$, in (31c), after which the optimization adhering to the convex constraints (31d) is conducted.

At each time step, the OCP (31) outputs a globally optimal input trajectory

$$\mathbf{U}_t^* = \left[\mathbf{u}_t^*(0)^\top, ..., \mathbf{u}_t^*(N_p-1)^\top\right]^\top,$$

where

$$\mathbf{u}_t^{*\top} = \left[P_{r,1}^*, P_{r,2}^*, P_{r,3}^*, P_g^*\right]^\top,$$

is applied to the wind turbine, in which $\mathbf{u}_t$ is a shorthand notation of $\mathbf{u}_t(0)$ with the asterisk symbol $(^*)$ indicating the optimal inputs. One may directly notice that $\mathbf{u}_t$ is not directly usable for wind turbine control; therefore, its equivalence in terms of the original variables

$$\mathbf{u}^{*\top} = \left[\beta_1^*, \beta_2^*, \beta_3^*, T_g^*\right]^\top,$$

must be retrieved by the following reverse transformations

$$\beta_i^* = \Psi\left(K_g^*, P_{r,i}^*, \hat{v}_i\right), \tag{32}$$

$$T_g^* = \frac{P_g^*}{\eta_g\left(\sqrt{2K_g^*/J_{hss}}\right)}, \tag{33}$$

where Ψ denotes the pitch look-up table[23] and K_g^*, with a slight abuse of notation, the prediction of the state K_g at $k=1$.

Remark 2. It is important to keep in mind that due to the model-plant mismatches from the model simplifications, limited data to construct coefficient tables, and mathematical manipulations for the convexification purposes, as described in the previous sections, the optimal solution resulting from solving the convex OCP (31) may not necessarily coincide with the global optimum of the real-world system. Still, it can be considered that the global optimality of the convex OCP with respect to the considered internal model and available measurement and estimation data is valid.

4.2 | Estimator designs

With regard to supplying the proposed controller with important but unknown and unmeasurable information, two estimators are designed. Firstly, the BEWS v_i, needed for constructing the aerodynamic power constraints (23), is not typically known from the measurements. However,

load-sensing technologies are available from the literature, in which the BEWS estimate $\hat{v}_i$ can be acquired from blade loads measurements.[27,33] In Section 4.2.1, the Coleman BEWS estimator design for such a purpose is described.[27] Secondly, discrepancies between the measured OoP blade root bending moments and that of the internal CEMPC-IPC model might deteriorate the performance of the blade loads mitigation in that low-frequent biases in the rotor tilt and yaw moments may appear and need to be compensated. Therefore, these unknown biases need to be estimated, in which an unscented Kalman filtering approach is adopted and discussed in Section 4.2.2.

4.2.1 | Coleman BEWS estimator

To estimate v_i, a recently developed load-sensing method, namely, the Coleman BEWS estimator, is employed[27] and briefly summarized hereunder. This estimation framework relies on the minimization of the error between the measured $M_{\text{op},i}$ and its estimate $\hat{M}_{\text{op},i}$ (with the hat symbol $\hat{(\cdot)}$ indicating estimated values)

$$\epsilon_i(t) = M_{\text{op},i}(t) - \hat{M}_{\text{op},i}(t), \tag{34}$$

in which

$$\hat{M}_{\text{op},i}(t) = \frac{1}{2}\rho A R C_{\text{m}}(\omega_{\text{r}}(t), \beta_i(t), \hat{v}_i(t), \psi_i(t))\hat{v}_i^2, \tag{35}$$

with C_{m} as the azimuth-dependent cone coefficient table. Similar to C_{p} and C_{t}, the values of C_{m} are collected from simulations using steady wind after the steady state is reached.

In this estimation scheme, ϵ_i is transformed into the fixed frame by a forward Coleman transformation, including the collective component $\epsilon_{\text{col}} = 1/3\sum_{i=1}^{3}\epsilon_i$, aside from the projection in the cosine and sine directions $\epsilon_{\text{tilt}} = 2/3\sum_{i=1}^{3}\epsilon_i \cos(\psi_i)$ and $\epsilon_{\text{yaw}} = 2/3\sum_{i=1}^{3}\epsilon_i \sin(\psi_i)$, respectively. The next step is to map these errors into the collective, tilt, and yaw components of the wind speed, $\hat{v}_{\text{col}}$, $\hat{v}_{\text{tilt}}$, and $\hat{v}_{\text{yaw}}$, respectively, by means of integration as follows:

$$\hat{v}_{\text{col}}(t) = \mathcal{K}_{\text{col}} \int_0^t \epsilon_{\text{col}}(\tau)\,\mathrm{d}\tau, \tag{36a}$$

$$\hat{v}_{\text{tilt}}(t) = \mathcal{K}_{\text{tilt}} \int_0^t \epsilon_{\text{tilt}}(\tau)\,\mathrm{d}\tau, \tag{36b}$$

$$\hat{v}_{\text{yaw}}(t) = \mathcal{K}_{\text{yaw}} \int_0^t \epsilon_{\text{yaw}}(\tau)\,\mathrm{d}\tau, \tag{36c}$$

where the constants $\mathcal{K}_{\text{col}}$ and $\mathcal{K}_{\text{tilt}} = \mathcal{K}_{\text{yaw}}$ are the corresponding integrator gains.

Following (36), a reverse Coleman transformation is utilized in order to project $\hat{v}_{\text{col}}$, $\hat{v}_{\text{tilt}}$, and $\hat{v}_{\text{yaw}}$ back into the rotating domain $\hat{v}_i$ as follows:

$$\hat{v}_i(t) = \hat{v}_{\text{col}}(t) + \hat{v}_{\text{tilt}}(t)\cos(\psi_i(t)) + \hat{v}_{\text{yaw}}(t)\sin(\psi_i(t)). \tag{37}$$

By feeding the above wind speed estimate (along with the measurements of ω_{r}, β_i, and ψ_i) into (35), $\hat{M}_{\text{op},i}$ is obtained and a feedback interconnection is created. Subsequently, due to the integrations in (36), the moment estimation errors are minimized, implying that $\hat{v}_i$ has been estimated. The interested reader is referred to the work of Liu et al.[27] for more elaborated explanations and derivations on the BEWS estimator.

4.2.2 | Biases estimation by unscented Kalman filtering

The utilization of the static modeling method as used in this study, in which aerodynamic coefficient tables are relied upon, may become one source of mismatches between the internal CEMPC-IPC model and the actual system. In addition, Assumptions 1–3 introduced earlier, as well as the differences between moment calculations in (11) and (35), may contribute further to these mismatches.

For the purpose of blade loads alleviation by the proposed method, the accuracy in the computations of M_{tilt} and M_{yaw} within the controller's internal model is of high importance. As the goal of the CEMPC-IPC is to mitigate blade loads, which is reflected predominantly as the 0P components in the rotor moments, it must be ensured that minimum static biases are exhibited with respect to the actual measurements, $M_{\text{tilt,m}}$ and $M_{\text{yaw,m}}$. Therefore, (27) and (28) need to be revised by including the corresponding biases $M_{\text{tilt,b}}$ and $M_{\text{yaw,b}}$ as follows:

$$M_{\text{tilt,m}}(t) = M_{\text{tilt}}(t) + M_{\text{tilt,b}}(t), \tag{38a}$$

$$M_{\text{yaw,m}}(t) = M_{\text{yaw}}(t) + M_{\text{yaw,b}}(t), \tag{38b}$$

with the information about these unknown biases to be provided by a state estimator. To this end, a recursive estimation routine by unscented Kalman filtering (UKF)[34] is considered, where the following random-walk model for estimating the unknown parameters is augmented to the original system dynamics (1)

$$M_{\text{tilt,b}}(k+1) = M_{\text{tilt,b}}(k) + q_{\text{tilt,b}}(k), \tag{39a}$$

$$M_{\text{yaw,b}}(k+1) = M_{\text{yaw,b}}(k) + q_{\text{yaw,b}}(k), \tag{39b}$$

with $q_{\text{tilt,b}}$ and $q_{\text{yaw,b}}$ being the process noises of the biases.

The nonlinear state and output equations internal of the UKF are defined as follows:

$$\begin{cases} \mathbf{x}_{\text{ukf}}(k+1) & = f_{\text{ukf}}(\mathbf{x}_{\text{ukf}}(k), \mathbf{u}_{\text{ukf}}(k)) + \mathbf{q}_{\text{ukf}}(k) \\ \mathbf{y}_{\text{ukf}}(k) & = h_{\text{ukf}}(\mathbf{x}_{\text{ukf}}(k), \mathbf{u}_{\text{ukf}}(k)) + \mathbf{r}_{\text{ukf}}(k) \end{cases}, \tag{40}$$

with

$$\begin{aligned} \mathbf{x}_{\text{ukf}}(k) &= \left[\omega_{\text{g}}(k), M_{\text{tilt,b}}(k), M_{\text{yaw,b}}(k)\right]^{\top}, \\ \mathbf{u}_{\text{ukf}}(k) &= \left[\beta_1(k), \beta_2(k), \beta_3(k), \hat{v}_1(k), \hat{v}_2(k), \hat{v}_3(k), T_{\text{g}}(k), \psi_1(k), \psi_2(k), \psi_3(k)\right]^{\top}, \\ \mathbf{y}_{\text{ukf}}(k) &= \left[\omega_{\text{g}}(k), M_{\text{tilt,m}}(k), M_{\text{yaw,m}}(k)\right]^{\top}, \\ \mathbf{q}_{\text{ukf}}(k) &= \left[q_{\omega_{\text{g}}}(k), q_{\text{tilt,b}}(k), q_{\text{yaw,b}}(k)\right]^{\top}, \\ \mathbf{r}_{\text{ukf}}(k) &= \left[r_{\omega_{\text{g}}}(k), r_{\text{tilt,m}}(k), r_{\text{yaw,m}}(k)\right]^{\top}, \end{aligned}$$

being the respective augmented state, input, output, process noise, and measurement noise vectors. Here, the noise terms are assumed to be zero-mean Gaussian random variables with covariances

$$\mathbf{Q}_{\text{ukf}} = \text{diag}\left(\sigma^2(q_{\omega_{\text{g}}}), \sigma^2(q_{\text{tilt,b}}), \sigma^2(q_{\text{yaw,b}})\right), \tag{41a}$$

$$\mathbf{R}_{\text{ukf}} = \text{diag}\left(\sigma^2(r_{\omega_{\text{g}}}), \sigma^2(r_{\text{tilt,m}}), \sigma^2(r_{\text{yaw,m}})\right), \tag{41b}$$

where σ represents the standard deviation of the indicated signal. The reader interested in the detailed procedure of UKF is referred to the literature.[34]

5 | SIMULATION RESULTS AND DISCUSSIONS

In this section, the main results of the proposed CEMPC-IPC design are exhibited in the aero-servo-elastic mid-fidelity wind turbine simulation environment NREL FAST v8.16.[28] As a representation of modern onshore wind turbines, the NREL-5 MW[35] reference turbine is chosen in this work, the main specifications of which are listed in Table 1[†]. Nine degrees of freedom (DOFs) are activated in FAST, including the generator DOF,

[†]The NREL-5 MW wind turbine used here is based on that included within FASTTool software package[36]; thus some parameters differ from the original version released by NREL.

TABLE 1 NREL 5-MW key specifications.

Description	Notation	Value	Unit
Rated generator power	$P_{g,rated}$	5	MW
Cut-in wind speed	v_{in}	4	m/s
Rated wind speed	v_{rated}	11.4	m/s
Cut-out wind speed	v_{out}	25	m/s
Rotor radius	R	63	m
Rotor area	A	12,468.98	m^2
Hub height	-	90	m
Optimal tip-speed ratio	$\lambda^\star$	7	-
Max. power coefficient	$C_p^\star$	0.458	-
Generator efficiency	η_g	0.944	-
Gearbox ratio	G	97	-
Generator inertia	J_g	534.116	kg/m^2
Rotor inertia	J_r	35,776,753	kg/m^2
HSS equivalent inertia	J_{hss}	4,336.512	kg/m^2
Rated generator speed	$\omega_{g,rated}$	1,173.7	rpm
Max. generator speed	$\omega_{g,max}$	1.3 $\omega_{g,rated}$	rpm
Rated generator torque	$T_{g,rated}$	43,093.55	Nm
Min. pitch angle	β_{min}	0	°
Max. pitch angle	β_{max}	25	°
Max./min. pitch rate	$\dot{\beta}_{max} = -\dot{\beta}_{min}$	8	°/s

Abbreviation: NREL, National Renewable Energy Laboratory.

drivetrain rotational-flexibility DOF, two fore-aft tower bending mode DOFs, two side-side tower bending mode DOFs, two flapwise blade bending mode DOFs, and the first edgewise blade bending mode DOF.

The CEMPC-IPC optimization is implemented using YALMIP modeling interface,[37] in which MOSEK[38] is incorporated as the numerical solver. For all of the simulations done for this section, the prediction horizon of $N_p = 100$ steps is considered with $T_s = 0.2$ s step size, such that 20 s of horizon length is obtained. For obtaining the required information on the BEWS and rotor moment biases, the Coleman estimator and UKF, briefly explained in Section 4, are tuned appropriately. The values of the Coleman BEWS estimator's integrator gains are set such that $\hat{v}_i$ can be obtained fast enough while maintaining a stable response as follows:

$$\mathcal{K}_{col} = 8.5 \cdot 10^{-7}\,(\mathrm{Ns})^{-1},\ \mathcal{K}_{tilt} = 10^{-6}\,(\mathrm{Ns})^{-1},\ \mathcal{K}_{yaw} = 10^{-6}\,(\mathrm{Ns})^{-1}.$$

The tuning parameters of the UKF, being the individual process and measurement noise covariances within the matrices $\mathbf{Q}_{ukf}$ and $\mathbf{R}_{ukf}$, are selected below

$$\begin{aligned}\sigma^2\left(q_{\omega_g}\right) &= 10^{-2}\,(\mathrm{rad/s})^2,\ \sigma^2(q_{\mathrm{tilt,b}}) = 10^{-2}\,(\mathrm{Nm})^2,\ \sigma^2(q_{\mathrm{yaw,b}}) = 10^{-2}\,(\mathrm{Nm})^2,\\ \sigma^2\left(r_{\omega_g}\right) &= 10^{-3}\,(\mathrm{rad/s})^2,\ \sigma^2(r_{\mathrm{tilt,m}}) = 10\,(\mathrm{Nm})^2,\ \sigma^2(r_{\mathrm{yaw,m}}) = 10\,(\mathrm{Nm})^2,\end{aligned}$$

such that the estimate signals $\hat{M}_{\mathrm{tilt,b}}$ and $\hat{M}_{\mathrm{yaw,b}}$ contain only slow-frequent components.

A number of deterministic and stochastic wind conditions are taken into consideration for studying the behavior and performance of the proposed controller, as well as comparison with the baseline controller. In Section 5.1, the former wind condition is chosen as a steady, stepped wind speed case to showcase the performance and differences of the CEMPC-IPC with respect to a basic CEMPC without any blade loads mitigation aspects. Then in Section 5.2, several turbulent wind conditions representing those of real-world scenarios are considered, in which its load reduction performance, as well as blade pitching activities, is assessed with respect to a baseline conventional IPC.

5.1 | Step wind

For the stepped wind case studied in this section, hub height wind speeds ranging between $v = 14$ and 20 m/s, with a 2 m/s increment every 60 s, are employed, totaling in a simulation duration of 300 s. The first few seconds of the simulation data commonly contain computational transients of FAST, and hence, the actual simulation duration is prolonged by 1 min such that these effects can be later removed during evaluation. To induce periodic $M_{\text{op},i}$ at the 1P frequency, which lies about $\omega_{\text{r,rated}} = \omega_{\text{g,rated}}/G = 12.1$ rpm or 0.2 Hz, wind shear power law[1] with 0.2 exponent value and tower shadow effect are taken into account in the FAST's setting. This periodic signal is reflected predominantly as static rotor moments in the tilt and yaw directions in the nonrotating frame, as indicated previously. Below-rated condition is disregarded from this simulation as operations in this region to avoid unnecessary acceleration in pitch motors wear and tear.

Several weight configurations, listed in Table 2, are considered to understand the behavior of the CEMPC-IPC under different prioritizations of economic objectives. Not all weights are relevant for load reduction, namely, $w_1 - w_3$ and w_5; thus, their values are fixed, whereas w_4, w_6, and w_7 are subject to changes later on in Sections 5.1.1 and 5.1.2. For all configurations, $w_1 = 100$, $w_2 = 50$, $w_3 = 10$, and $w_5 = 50$ are set. The weight w_1 is set to enforce the production of $P_{\text{g}} = P_{\text{g,rated}}$ during the operation at above-rated. The $\check{P}_{\text{av},i}$ maximization weight w_2 is chosen to push the upper bound of (23), thereby expanding the range within which the decision variable $P_{\text{r},i}$ may find its optimal value. As for w_3, the chosen value is sufficient to regulate K_{g} whenever the generator excurses to kinetic energies higher than $K_{\text{g,rated}}$ by lowering P_{r} (see (5)), which is realized by increasing the collective pitch component of the blades. Under these weights for power control and speed regulation, comparisons between the proposed CEMPC-IPC and a basic CEMPC, as well as demonstrations of CEMPC-IPC behaviors under different w_4, w_6, and w_7 tuning, are conducted in the subsequent subsections.

5.1.1 | CEMPC-IPC and basic CEMPC comparison

In this subsection, the behavior of the proposed controller without and with load reduction is compared. The former resembles that of the original CEMPC,[23] with the exception that neither local storage nor grid power delivery is considered for the sake of simplicity, which is obtained by a slight modification of the latter. The main modification is in the replacement of the v_i into rotor-effective wind speed (REWS) estimate $\hat{v}_{\text{RE}} = \sum_{i=1}^{3} \hat{v}_i/3$. This is required to enforce equal $P_{\text{r},i}$ for all blades, which, after variable conversion into β_i by the reverse pitch LUT Ψ in (32), results in collective pitching. No penalties on M_{tilt} and M_{yaw} are imposed in the CEMPC setting, that is, $w_6 = w_7 = 0$, to prevent individual pitching of this controller despite the use of $\hat{v}_{\text{RE}}$, since it is still possible to induce modest individual pitch activities as done for side-side tower damping.[26] As for the CEMPC-IPC, $\hat{v}_i$ is re-utilized and the load mitigation weights for penalizing M_{tilt} and M_{yaw} are set to $w_6 = w_7 = 100$ so that $P_{\text{r},i}$ can now actively steer these moments closer to 0 Nm. For both CEMPC and CEMPC-IPC, listed as Configuration 1 and Configuration 2 in Table 2, respectively, a fixed penalty on $\dot{P}_{\text{r},i}$, that is, $w_4 = 50$ is selected. Figure 3 depicts the time-marching results of both the basic CEMPC (black lines) and CEMPC-IPC (red lines) under these configurations, with all blade-effective quantities only shown for the first blade, for the sake of clarity.

As shown in the figure, the basic CEMPC under Configuration 1 does not perform any individual pitching, as β_1 acts collectively with β_2 and β_3 only for speed regulation due to zero weights on w_6 and w_7, as well as the utilization of v_{RE}. Also depicted is $P_{\text{r},1}$ of the basic CEMPC, which appears to maintain its value of about 1.65–1.85 MW as a realization of an active overspeeding penalty. Under this benchmark configuration, the first OoP blade root bending moment $M_{\text{op},1}$ experiences severe 1P loading in the rotating reference frame due to the wind shear and tower shadow effects, which, as the wind becomes faster, becomes more significant. Considerable deviation of the static components of M_{tilt} and M_{yaw} from 0 Nm is thus observed in the fixed frame as a consequence of this 1P load in the rotating frame. In comparison with CEMPC-IPC under Configuration 2, improvements in terms of fatigue load reduction are evident from the measurements of $M_{\text{op},1}$, where fewer 1P oscillation are experienced. Consequently, M_{tilt} and M_{yaw} exhibit much less static loading compared to the previous configuration.

5.1.2 | CEMPC-IPC behavior under different aerodynamic power rate penalties

Another aspect worth paying attention to is the CEMPC-IPC load reduction behavior under different penalties on $\dot{P}_{\text{r},i}$, which is considered in this subsection. In a previous work,[26] penalizing $\dot{P}_{\text{r},i}$ was shown as a way to prevent excessive individual pitching, which consequently results in less tower load mitigation activity. To study how the penalization of $\dot{P}_{\text{r},i}$ is affecting the blade loads in the current work, additional step wind simulations are performed, in which two different weight configurations for CEMPC-IPC are set, that is, Configuration 3 and Configuration 4. In the former and latter configurations, respectively, $w_4 = 100$ and $w_4 = 25$ are selected, representing high and low penalties on the $\dot{P}_{\text{r},i}$, with the tilt and yaw moment penalties are set equally to $w_6 = w_7 = 10$. Figure 4 depicts the time-marching simulation results for both cases, where, for the sake of clarity, only an excerpt of the measurements at $t = 175$–275 s is shown.

TABLE 2 CEMPC-IPC weight configurations for step wind case.

Configuration	w_1	w_2	w_3	w_4	w_5	w_6	w_7
1 (Basic CEMPC)	100	50	10	**50**	50	**0**	**0**
2	100	50	10	**50**	50	**100**	**100**
3	100	50	10	**100**	50	**10**	**10**
4	100	50	10	**25**	50	**10**	**10**

Note: Weights description: w_1: generator power maximization; w_2: available power maximization; w_3: overspeeding penalty; w_4: aerodynamic power rate-of-change penalty; w_5: generator power rate-of-change penalty; w_6: tilt moment penalty; w_7: yaw moment penalty. Bold numbers indicate varied weights.
Abbreviations: CEMPC, convex EMPC; IPC, individual pitch control.

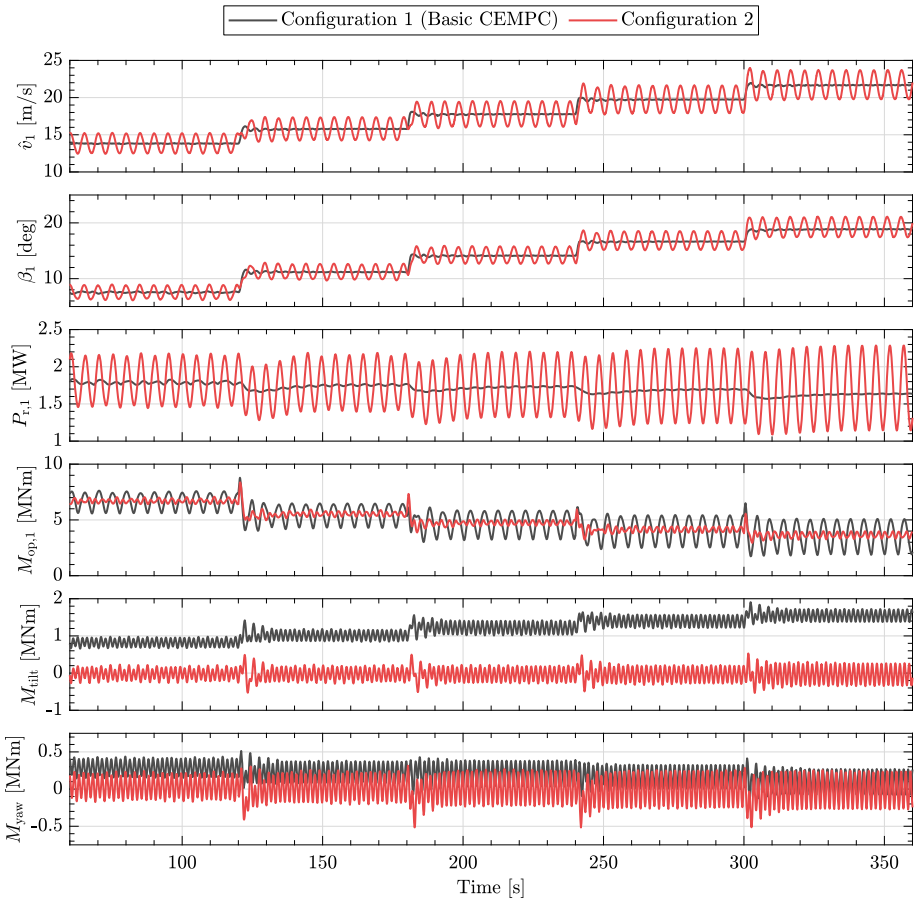

FIGURE 3 Step wind case time-marching simulation results of basic convex EMPC (CEMPC) under Configuration 1 and CEMPC-individual pitch control (IPC) under Configuration 2.

In the figure, CEMPC-IPC with Configuration 4 (red lines) clearly shows more active $P_{r,i}$ than Configuration 3 (black lines). This behavior is anticipated since w_4 is decreased in the former configuration, which enables $P_{r,i}$ to vary with higher magnitude. This results in β_i with slightly smaller oscillation but with reduced $M_{op,i}$. The reduction in the blade loads is, again, reflected as a reduction in the static components of M_{tilt} and M_{yaw}, as evident in the figure. Such an observation might be counterintuitive as one might expect that decreased w_4 would give more aggressive pitching, as was demonstrated in the previous work.[26] Under constant $\hat{v}_i$ (in that it does not vary periodically in 1P frequency) and constant K_g at above-rated, as considered in the previous work, one may find that a high $P_{r,i}$ variation also translates to a high variation of β_i computed by Ψ. This is not the case here since $\hat{v}_i$, being a varying signal at 1P due to the wind shear and tower shadow, has more influence on the computation of β_i, along with $P_{r,i}$ and K_g, which in the end creates lower β_i variation. Having the knowledge of such behavior at hand, trade-off tuning between pitch activities and load mitigation, being parts of the economic objectives of CEMPC-IPC, can thus be applied appropriately for other conditions, such as the following turbulence cases.

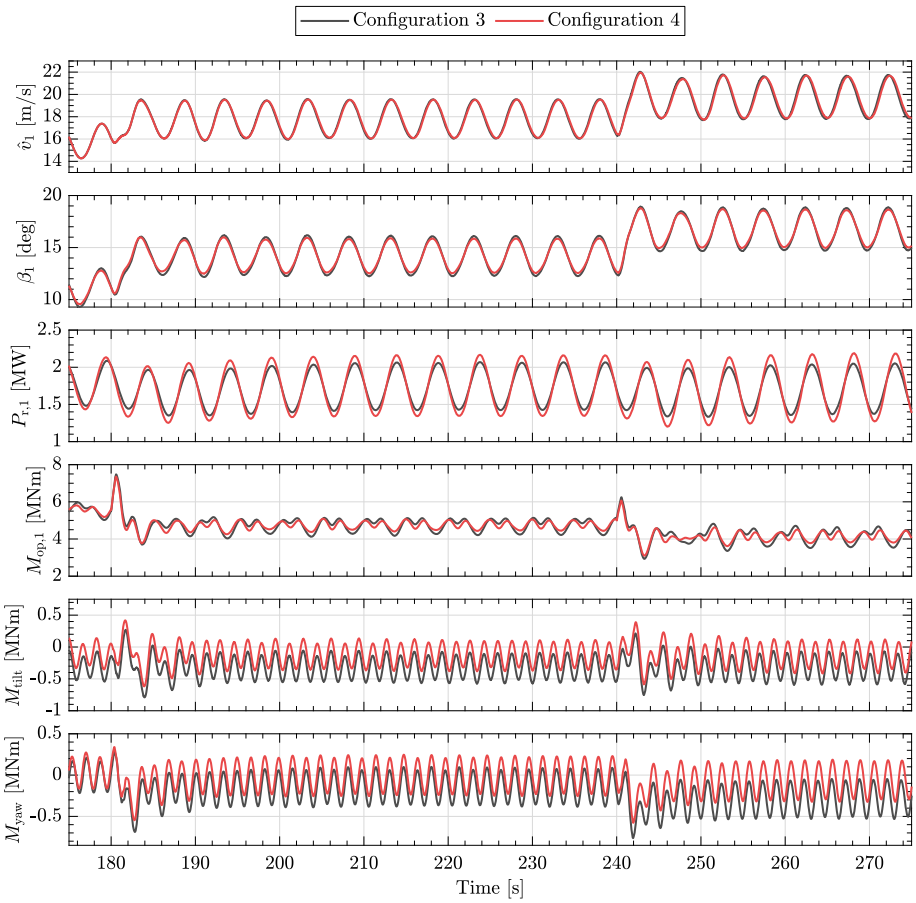

FIGURE 4 Step wind case time-marching simulation results of convex EMPC (CEMPC)-individual pitch control (IPC) under Configuration 3 and Configuration 4.

TABLE 3 CEMPC-IPC weight configurations for turbulent wind cases.

Configuration	Turbulence case	w_1	w_2	w_3	w_4	w_5	w_6	w_7
1	$v_0 = 20$ m/s, $I_T = 16\%$	100	50	10	**100**	50	**50**	**50**
2	$v_0 = 20$ m/s, $I_T = 8\%$	100	50	10	**50**	50	**75**	**75**
3	$v_0 = 16$ m/s, $I_T = \{12,16\}\%$ and $v_0 = 20$ m/s, $I_T = 12\%$	100	50	10	**20**	50	**90**	**90**
4	$v_0 = 16$ m/s, $I_T = \{4,8\}\%$ and $v_0 = 20$ m/s, $I_T = 4\%$	100	50	10	**10**	50	**95**	**95**

Note: Weights description: w_1: generator power maximization; w_2: available power maximization; w_3: overspeeding penalty; w_4: aerodynamic power rate-of-change penalty; w_5: generator power rate-of-change penalty; w_6: tilt moment penalty; w_7: yaw moment penalty. Bold numbers indicate varied weights.
Abbreviations: CEMPC, convex EMPC; IPC, individual pitch control.

5.2 | Turbulent wind

In this case, several turbulent wind fields generated by NREL TurbSim[39] with the Kaimal turbulence model defined in the IEC 61400-3 standard[40] are employed, including wind shear and tower shadow as used previously. Two mean wind speeds at hub height are considered, namely, $v_0 = 16$ m/s and $v_0 = 20$ m/s, where, for each mean speed, turbulence levels of $I_T = \{4,8,12,16\}\%$ are simulated, making up of eight turbulence cases in total. For each turbulence case, a 660 s long simulation is run, from which only the last 600 s is evaluated such that FAST computational transients are not accounted for.

The tuning weights of the CEMPC-IPC in the current performance study are set on a case-per-case basis, taking into account the trade-off between loads reduction and pitch activities according to the observations from the previous wind case. These weights, tuned accordingly for each wind speed and turbulence condition, are provided in Table 3.

The performance of CEMPC-IPC in the current turbulent scenarios is compared with a baseline conventional Coleman-based IPC,[2,4] operating alongside a standard K-omega-squared controller and gain-scheduled collective pitch control (CPC) for torque control and rotational speed regulation, respectively.[41] The conventional IPC employed in this work is a pair of pure integrators with equal gains $K_{I,tilt} = K_{I,yaw} = 2.6604 \cdot 10^{-9}$ rad/Nm, for canceling out the static components of rotor moments M_{tilt} and M_{yaw}, as computed in (14) and (15). The gains are chosen based on the frequency domain loop-shaping method so as to obtain 0.15 rad/s crossover frequency. The pitch demands β_{tilt} and β_{yaw} generated by these integrators in the fixed frame, together with the collective pitch signal β_{col} used in CPC, are reconstructed into β_i, by the following reverse Coleman transformation

$$\beta_i(t) = \beta_{col}(t) + \beta_{tilt}(t)\cos(\psi_i(t) + \psi_{off}) + \beta_{yaw}(t)\sin(\psi_i(t) + \psi_{off}), \tag{42}$$

with ψ_{off} being an azimuth offset to compensate for the coupling between the tilt and yaw axes. For the considered operating points, $\psi_{off} = 17.5^\circ$ is chosen such that the cross-coupling between the tilt and yaw axes is minimized. As the integrator gains needed to reach the aforementioned crossover frequency, as well as the azimuth offset for decoupling both fixed axes, do not vary too much at the above-rated, a gain-scheduling strategy is deemed unnecessary. The reader interested in the detailed implementation of the baseline IPC with azimuth offset inclusion as a decoupling strategy is referred to the work of Mulders et al.[4]

A number of performance indicators are used for assessing the load reduction quality and also blade pitching activities for the baseline controller, without and with IPC, and the designed CEMPC-IPC as follows:

1. Mean standard deviation of OoP blade root bending moments

$$\sigma_{M_{op,123}} = \sum_{i=1}^{3} \sigma(M_{op,i})/3,$$

2. Standard deviation of the low-speed-shaft (LSS) bending moment in the rotating frame

$$\sigma_{M_{lss}} = \sigma(M_{lss}),$$

3. Standard deviation of the yaw bearing yaw moment in the fixed frame

$$\sigma_{M_{yb}} = \sigma(M_{yb}),$$

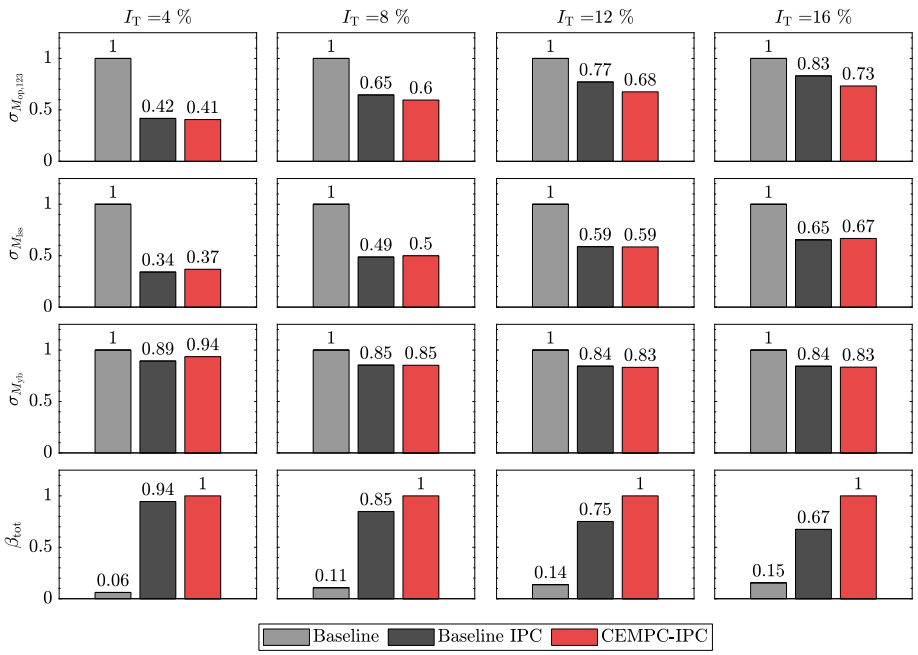

FIGURE 5 Normalized bending moments standard deviations of multiple wind turbine components and cumulative pitch travel for turbulence cases for mean hub height wind speed $v_0 = 16$ m/s.

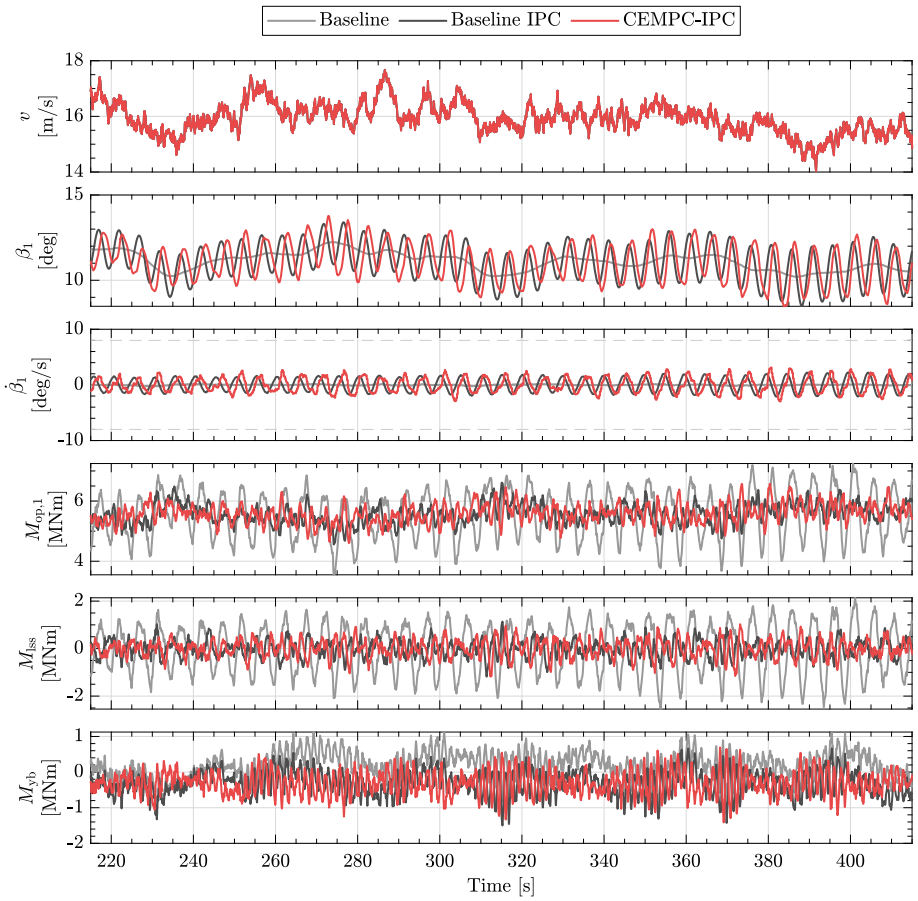

FIGURE 6 Excerpt of the time series simulation results of $v_0 = 16$ m/s for $I_T = 4\%$ at $t = 215$–415 s.

4. Cumulative pitch distance traveled by the blades[42]

$$\beta_{\text{tot}} = \sum_k \sum_{i=1}^{3} |\Delta\beta_i(k)|,$$

where $\Delta\beta_i(k) = \beta_i(k) - \beta_i(k-1)$.

The moments considered in the standard deviations represent those of the actual wind turbine components, where load sensors are installed in the field,[2,42,43] in contrast to M_{tilt} and M_{yaw}, which are projections of $M_{\text{op,i}}$ and not from actual components. Note that since simulation data of only 10 min for each turbulence case are considered, therefore, standard deviations of load measurements are preferred to evaluate the damage reduction of different wind turbine components[‡].

The performance indicators data computed for all of the turbulence cases are collected in Table A1 in Appendix A, where, for convenience, their normalized values are depicted as comparative bar graphs in Figure 5 for $v_0 = 16$ m/s. In the figure, the standard deviations of the aforementioned bending moments and β_{tot} are normalized with respect to either the baseline controller without IPC or CEMPC-IPC, where appropriate, for better readability of the bar heights. Since similar conclusions can be drawn for turbulent cases of $v_0 = 20$ m/s, their bar graphs are not presented for brevity.

In Figure 5, some trends in the load reduction performance of the CEMPC-IPC at $v_0 = 16$ m/s can be observed. It is apparent that, generally, similar performance in the reduction of the $\sigma_{M_{\text{lss}}}$ and $\sigma_{M_{\text{yb}}}$ with respect to the baseline IPC is attained by the CEMPC-IPC for all turbulence intensities. More interestingly, as the turbulence intensity goes higher, the proposed controller performs better than the baseline IPC in terms of

[‡]For a more accurate assessment, damage equivalent load may also be employed; however, this requires more simulation data, thus, for simplicity is not considered in the current work.

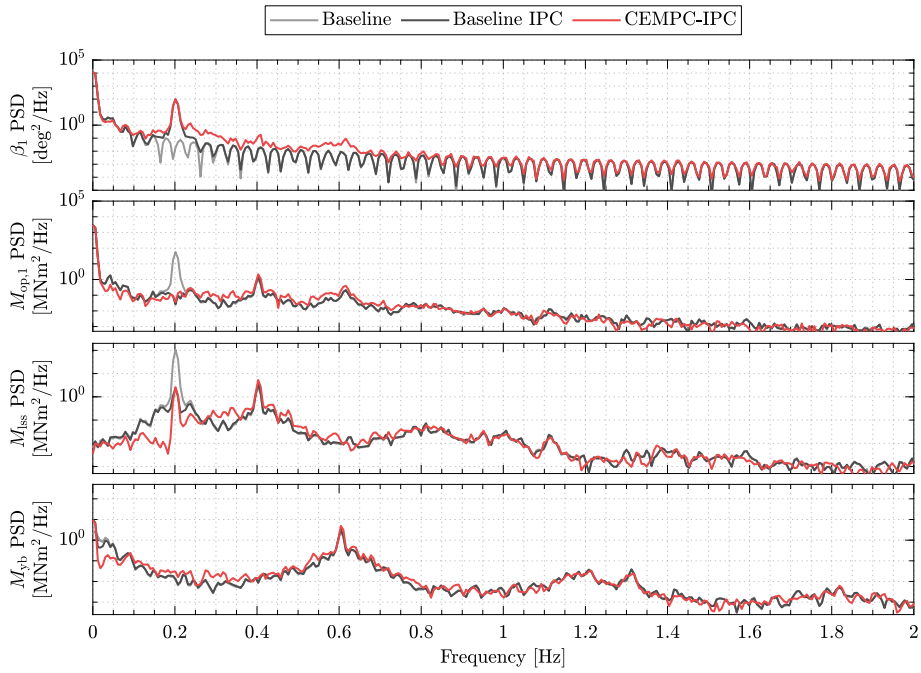

FIGURE 7 Power spectral density results for various wind turbine components of $v_0 = 16$ m/s for $I_T = 4\%$.

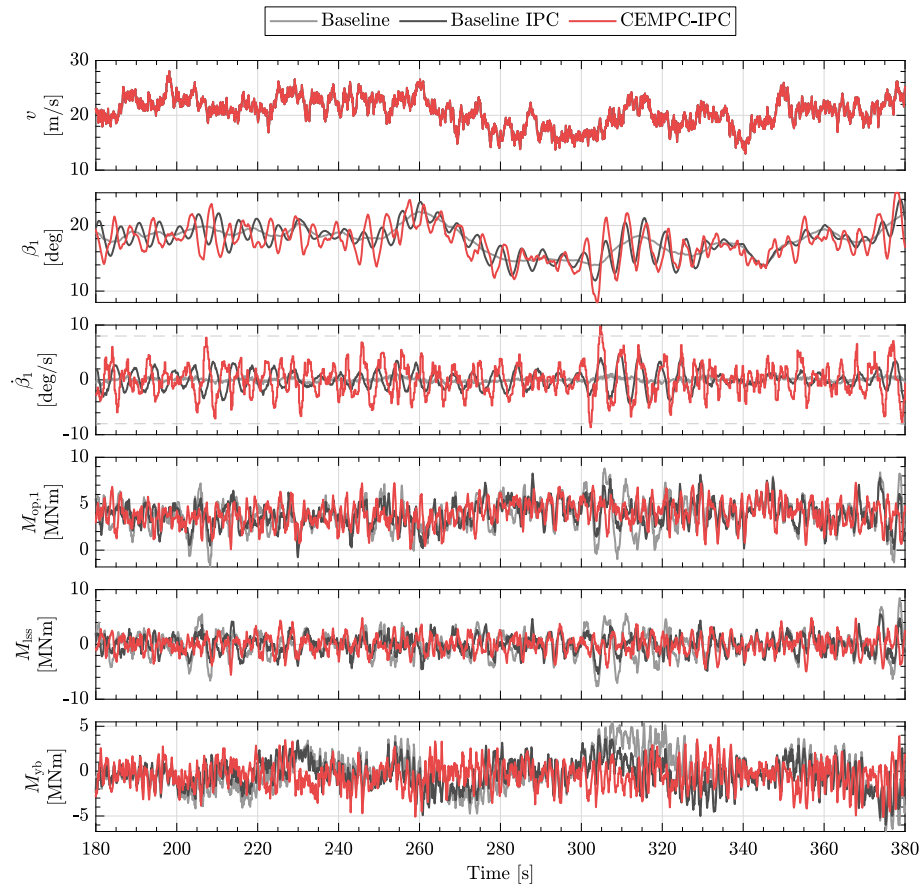

FIGURE 8 Excerpt of the time series simulation results of $v_0 = 20$ m/s for $I_T = 16\%$ at $t = 180$–380 s.

reduction in $\sigma_{M_{op,123}}$, from only 1% lower at $I_T = 4\%$ to 10% lower at $I_T = 16\%$. These improvements are linked with the increase in the pitch activities indicated by β_{tot} ranging from 6% to 33% higher than the baseline IPC.

Excerpts of time series results for both $v_0 = 16$ m/s and $v_0 = 20$ m/s wind speeds are provided, in which the records of v at hub height, β_1, $\dot{\beta}_1$, $M_{op,1}$, M_{lss}, and M_{yb} measurements are shown. In Figure 6, results from the scenario $v_0 = 16$ m/s under a low-turbulence case of $I_T = 4\%$ are depicted. It is shown that both the proposed CEMPC-IPC (red lines) and baseline IPC (black lines) are able to significantly reduce the fatigue loads $M_{op,1}$, M_{lss}, and M_{yb} experience with respect to those of by the baseline controller (gray lines). Similar pitching activities are seen between both IPC controllers, with slightly higher $\dot{\beta}_1$ for CEMPC-IPC, which shows consistency with β_{tot} evaluation indicated by the bar graphs in Figure 5. Also shown are the pitch rate limits $\dot{\beta}_{max} = -\dot{\beta}_{min} = 8^\circ/s$ as straight, dashed gray lines, which are not exceeded by both IPC controllers.

In Figure 7, the power spectral density (PSD) results of β_1, $M_{op,1}$, M_{lss}, and M_{yb} from the same turbulence case are presented, which are obtained based of Welch's power spectrum estimation method.[44] From the figure, a visible reduction in the 1P component of $M_{op,1}$ at 0.2 Hz can be clearly seen for both the CEMPC-IPC and baseline IPC, with the former method also resulting in a reduction at lower frequencies. In the measurements of the rotating M_{lss}, the 1P component in the signals can be better observed due to the low-frequent load components of the blades canceling each other out. Here, the reduction of the 1P loads is more evident, with the low-frequency contents between 0.1 and 0.2 Hz being further lowered by the CEMPC-IPC. However, the increase in the spectral densities at frequencies surrounding 0.3 Hz counterbalances the reduction obtained at the lower frequencies, which may explain why $\sigma_{M_{lss}}$ of this controller is close to that of the baseline IPC, as shown in Figure 5. The PSD results of β_1 indicate consistency with β_{tot} evaluated previously, in the sense that CEMPC-IPC exercises higher pitching activities with respect to the baseline IPC, particularly between 1P and 0.65 Hz.

In Figure 8, time domain signals for the case $v_0 = 20$ m/s with $I_T = 16\%$ are depicted. Here, the CEMPC-IPC again showcases its capability in reducing the loads experienced by $M_{op,1}$, as well as M_{lss} and M_{yb}, for instance, at $t = 200$–220 s and $t = 300$–320 s. The pitch system of the proposed controller is also more active as the turbulence level becomes higher. At times, $\dot{\beta}i$ might violate the pitch rate limits as shown between $t = 300$ and 310 s, since the current implementation of the CEMPC-IPC does not take into account explicitly pitch rate constraints; thus, room for future improvement.

Figure 9 illustrates the PSDs of the simulation results for the same turbulence case, from which a conclusion similar to that of the previous case's PSDs can be drawn. One noticeable difference is in the increase of the spectral content of β_1 for frequencies of about 0.1 Hz until approximately 1 Hz. This can be explained as follows. The increase in turbulence level is reflected as an increase in the overall frequency components in the wind. This information is carried over into the CEMPC-IPC via $\hat{v}_i$, which is also utilized by Ψ to obtain the optimal pitch angles, thereby giving rise to the pitch spectral content. This might also explain the necessity to use different weight combinations for different turbulence levels to obtain comparable results with respect to the baseline IPC. Investigating further the effects of different Coleman BEWS tuning parameters on the CEMPC-IPC weighting may be of interest for future study.

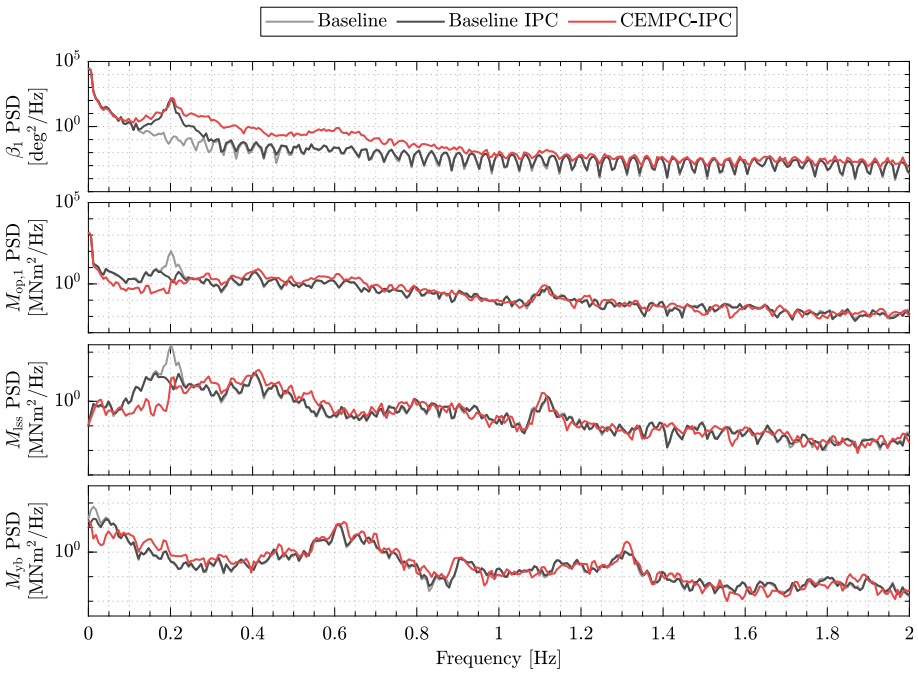

FIGURE 9 Power spectral density results for various wind turbine components of $v_0 = 20$ m/s for $I_T = 16\%$.

In light of the presented results, the CEMPC-IPC appears to perform comparably to the baseline IPC. However, this work is preliminary and mainly aimed at extending the fatigue loads mitigation capability of the CEMPC framework,[23,26] with a focus on blade loads. Improvements to maximize the potential of CEMPC-IPC may be achieved in future work, for instance, by augmenting a more accurate internal model and including a preview wind information so that better predictive capability of the controller can be attained. Another aspect worth looking for is the inclusion of pitch rate constraints to have better handling of the pitch drive mechanism.

6 | CONCLUSIONS

In this paper, a novel CEMPC-IPC method has been developed with blade loads alleviation capability, thereby extending the family of CEMPC controllers for wind turbine applications. The convexity of the proposed controller is made possible by the reformulation of a simplified wind turbine model in terms of power and energy flows, such that linear dynamics, convex constraints, and concave objective functions (to be maximized), embodied in an OCP, are obtained. Having such a convex OCP formulated, a globally optimal solution (with respect to the internal model and available measurement and estimation data) is guaranteed and real-time deployment becomes possible. The individual pitching capability of this framework is unlocked by the utilization of multiple aerodynamic powers—each representing that of an individual blade, in contrast to employing a single, rotor-effective quantity. Such individual aerodynamic powers are then used to substitute nominal turbine variables in the static blade forces and moments formulation. By including moment penalizations as part of the OCP's economic objectives, the pitching movement of the individual blades can now be controlled to mitigate wind turbine blade loads. Moreover, the proposed framework allows for trade-off tuning between different economic objectives with ease. For supplying unknown and unmeasurable information into the CEMPC-IPC, the load-sensing Coleman BEWS estimator and UKF moment biases estimator have been incorporated. Numerical simulations under the mid-fidelity NREL FAST environment have been conducted, both in step wind and turbulent wind cases, in which the performance of the CEMPC-IPC has been evaluated. Compared with a conventional IPC, the proposed method has been shown to yield similar performance in terms of mitigating OoP blade root bending moments, as well as rotating LSS and fixed yaw bearing yaw moments. The load-reducing capability of the proposed CEMPC-IPC thus, in conclusion, has shown the potential to prolong wind turbine lifetime, such that further economic benefit from its power-generating operations can be gained. To push the limit of the novel CEMPC-IPC, future work may consider improvements in internal model accuracy, incorporation of preview wind information, and incorporation of pitch rate constraints for better handling of pitching activities.

ACKNOWLEDGEMENTS

The authors have nothing to report.

CONFLICT OF INTEREST STATEMENT

This project has been conducted in cooperation with Vestas Wind Systems A/S.

PEER REVIEW

The peer review history for this article is available at https://www.webofscience.com/api/gateway/wos/peer-review/10.1002/we.2869.

DATA AVAILABILITY STATEMENT

Data are available on request from the authors.

ORCID

Atindriyo Kusumo Pamososuryo https://orcid.org/0000-0002-9037-043X
Yichao Liu https://orcid.org/0000-0002-4175-7638
Riccardo Ferrari https://orcid.org/0000-0003-3615-5445
Jan-Willem van Wingerden https://orcid.org/0000-0003-3061-7442

REFERENCES

1. Burton T, Jenkins N, Sharpe D, Bossanyi E. *Wind Energy Handbook*: Wiley; 2011.
2. Bossanyi EA. Individual blade pitch control for load reduction. *Wind Energy*. 2003;6(2):119-128. https://doi.org/10.1002/we.76
3. Bir G. Multi-blade coordinate transformation and its application to wind turbine analysis. In: *46th AIAA Aerospace Sciences Meeting and Exhibit*. https://doi.org/10.2514/6.2008-1300
4. Mulders SP, Pamososuryo AK, Disario GE, van Wingerden JW. Analysis and optimal individual pitch control decoupling by inclusion of an azimuth offset in the multiblade coordinate transformation. *Wind Energy*. 2019;22(3):341-359. https://doi.org/10.1002/we.2289
5. Stol KA, Zhao W, Wright AD. Individual blade pitch control for the controls advanced research turbine (CART). *J Solar Energy Eng*. 2006;128(4):498-505. https://doi.org/10.1115/1.2349542

6. Selvam K, Kanev S, van Wingerden JW, van Engelen T, Verhaegen M. Feedback-feedforward individual pitch control for wind turbine load reduction. *Int J Robust Nonlinear Control*. 2009;19(1):72-91. https://doi.org/10.1002/rnc.1324
7. Sandquist F, Moe G, Anaya-Lara O. Individual pitch control of horizontal axis wind turbines. *J Offshore Mech Arctic Eng-Trans ASME*. 2012;134(3): 31901. https://doi.org/10.1115/1.4005376
8. Geyler M, Caselitz P. Robust multivariable pitch control design for load reduction on large wind turbines. *J Solar Energy Eng*. 2008;130(3):31014. https://doi.org/10.1115/1.2931510
9. Lu Q, Bowyer R, Jones BL. Analysis and design of Coleman transform-based individual pitch controllers for wind-turbine load reduction. *Wind Energy*. 2015;18(8):1451-1468. https://doi.org/10.1002/we.1769
10. Vali M, van Wingerden JW, Kühn M. Optimal multivariable individual pitch control for load reduction of large wind turbines. In: 2016 American Control Conference (ACC); 2016:3163-3169. https://doi.org/10.1109/ACC.2016.7525404
11. Rawlings JB, Mayne DQ, Diehl M. *Model Predictive Control: Theory, Computation, and Design*, Vol. 2: Nob Hill Publishing Madison, WI; 2017.
12. Rawlings JB. Tutorial overview of model predictive control. *IEEE Control Syst*. 2000;20(3):38-52. https://doi.org/10.1109/37.845037
13. Friis J, Nielsen E, Bonding J, Adegas FD, Stoustrup J, Odgaard PF. Repetitive model predictive approach to individual pitch control of wind turbines. In: Conference on Decision and Control; 2011:3664-3670.
14. Henriksen LC, Hansen MH, Poulsen NK. Wind turbine control with constraint handling: a model predictive control approach. *IET Control Theory Appl*. 2012;6(11):1722-1734. https://doi.org/10.1049/iet-cta.2011.0488
15. Madsen M, Filsø J, Soltani M. Preview-based asymmetric load reduction of wind turbines. In: 2012 IEEE International Conference on Control Applications 2012 IEEE International Conference on Control Applications CCA); 2012:1424-1429.
16. Koerber A, King R. Combined feedback–feedforward control of wind turbines using state-constrained model predictive control. *IEEE Trans Control Syst Technol*. 2013;21(4):1117-1128. https://doi.org/10.1109/TCST.2013.2260749
17. Schlipf D, Schlipf DJ, Kühn M. Nonlinear model predictive control of wind turbines using LIDAR. *Wind Energy*. 2013;16(7):1107-1129. https://doi.org/10.1002/we.1533
18. Evans MA, Cannon M, Kouvaritakis B. Robust MPC tower damping for variable speed wind turbines. *IEEE Trans Control Syst Technol*. 2015;23(1):290-296. https://doi.org/10.1109/TCST.2014.2310513
19. Gros S. An economic NMPC formulation for wind turbine control. In: Proceedings of the IEEE Conference on Decision and Control; 2013:1001-1006. https://doi.org/10.1109/CDC.2013.6760013
20. Rawlings JB, Angeli D, Bates CN. Fundamentals of economic model predictive control. In: 2012 IEEE 51st IEEE Conference on Decision and Control (CDC). IEEE 2012 IEEE 51st IEEE Conference on Decision and Control (CDC); 2012:3851-3861.
21. Gros S, Schild A. Real-time economic nonlinear model predictive control for wind turbine control. *Int J Control*. 2017;90(12):2799-2812. https://doi.org/10.1080/00207179.2016.1266514
22. Mulders SP, Hovgaard TG, Grunnet JD, van Wingerden JW. Preventing wind turbine tower natural frequency excitation with a quasi-LPV model predictive control scheme. *Wind Energy*. 2020;23(3):627-644. https://doi.org/10.1002/we.2447
23. Hovgaard TG, Boyd S, Jørgensen JB. Model predictive control for wind power gradients. *Wind Energy*. 2015;18(6):991-1006. https://doi.org/10.1002/we.1742
24. Shaltout ML, Ma Z, Chen D. An adaptive economic model predictive control approach for wind turbines. *J Dyn Syst Meas Control*. 2018;140(5):1-10. https://doi.org/10.1115/1.4038490
25. Feng Z, Gallo AJ, Liu Y, Pamosoruyo AK, Ferrari RMG, van Wingerden JW. An economic model predictive control approach for load mitigation on multiple tower locations of wind turbines. In: 2022 IEEE 61st IEEE Conference on Decision and Control (CDC); 2022:2425-2430.
26. Pamosoruyo AK, Liu Y, Hovgaard TG, Ferrari R, van Wingerden JW. Individual pitch control by convex economic model predictive control for wind turbine side-side tower load alleviation. In: TORQUE 2022; 2022.
27. Liu Y, Pamosoruyo AK, Mulders SP, Ferrari RMG, van Wingerden JW. The proportional integral notch and Coleman blade effective wind speed estimators and their similarities. *IEEE Control Syst Lett*. 2022;6:2198-2203. https://doi.org/10.1109/LCSYS.2021.3140171
28. Jonkman BJ, Jonkman JM. FAST v8.16.00a-bjj user's guide, Colorado, USA, National Renewable Energy Lab.(NREL), Golden, CO (United States); 2016.
29. Lio WH. *Blade-Pitch Control for Wind Turbine Load Reductions*, Springer Theses. Cham: Springer International Publishing; 2018.
30. Raach S, Schlipf D, Sandner F, Matha D, Cheng PW. Nonlinear model predictive control of floating wind turbines with individual pitch control. In: American Control Conference; 2014:4434-4439.
31. Jain A, Schildbach G, Fagiano L, Morari M. On the design and tuning of linear model predictive control for wind turbines. *Renew Energy*. 2015;80:664-673. https://doi.org/10.1016/j.renene.2015.02.057
32. Åström KJ, Wittenmark B. *Computer-Controlled Systems: Theory and Design*: Courier Corporation; 2013.
33. Liu Y, Pamosoruyo AK, Ferrari R, Hovgaard TG, van Wingerden JW. Blade effective wind speed estimation: a subspace predictive repetitive estimator approach. In: 2021 European Control Conference (ECC); 2021:1205-1210.
34. Wan EA, Van Der Merwe R. The unscented Kalman filter for nonlinear estimation. In: IEEE 2000 Adaptive Systems for Signal Processing, Communications, and Control Symposium; 2000:153-158.
35. Jonkman J, Butterfield S, Musial W, Scott G. Definition of a 5-MW reference wind turbine for offshore system development, Colorado, USA, National Renewable Energy Lab.(NREL), Golden, CO (United States); 2009.
36. Mulders SP, Zaaijer MB, Bos R, van Wingerden JW. Wind turbine control: Open-source software for control education, standardization and compilation. *J Phys Conf Ser*. 2020;1452(1):12010. https://doi.org/10.1088/1742-6596/1452/1/012010
37. Löfberg J. YALMIP: a toolbox for modeling and optimization in matlab. In: 2004 IEEE International Conference on Robotics and Automation 2004 IEEE International Conference on Robotics and Automation; 2004:284-289.
38. ApS M. The MOSEK optimization toolbox for MATLAB manual. version 9.0.OSEK ApS. Denmark; 2019.
39. Jonkman BJ. Turbsim user's guide v2.00.00, Colorado, USA, National Renewable Energy Lab.(NREL), Golden, CO (United States); 2016.
40. IEC 61400-3 wind turbines part 3: design requirements for offshore wind turbines. *Standard*, Geneva, Switzerland, International Electrotechnical Commission; 2009.
41. Bossanyi EA. The design of closed loop controllers for wind turbines. *Wind Energy*. 2000;3(3):149-163. https://doi.org/10.1002/we.34

42. van Solingen E, van Wingerden JW. Linear individual pitch control design for two-bladed wind turbines. *Wind Energy*. 2015;18(4):677-697. https://doi.org/10.1002/we.1720
43. Bossanyi EA, Fleming PA, Wright AD. Validation of individual pitch control by field tests on two-and three-bladed wind turbines. *IEEE Trans Control Syst Technol*. 2013;21(4):1067-1078. https://doi.org/10.1109/TCST.2013.2258345
44. Welch P. The use of fast Fourier transform for the estimation of power spectra: a method based on time averaging over short, modified periodograms. *IEEE Trans Audio Electroacoustics*. 1967;15(2):70-73. https://doi.org/10.1109/TAU.1967.1161901

How to cite this article: Pamososuryo AK, Liu Y, Gybel Hovgaard T, Ferrari R, van Wingerden J-W. Convex economic model predictive control for blade loads mitigation on wind turbines. *Wind Energy*. 2023;26(12):1276-1298. doi:10.1002/we.2869

APPENDIX A: TURBULENT WIND CASE SIMULATION RESULTS

TABLE A1 Baseline controllers and CEMPC-IPC results in moment standard deviations and cumulative pitch travel distance.

v_0 (m/s)	16				20			
I_T (%)	4	8	12	16	4	8	12	16
Mean standard deviation of OoP blade root bending moments $(\sigma_{M_{op,123}})$								
Baseline (kNm)	841.420	1061.333	1372.230	1726.434	1078.221	1286.137	1589.222	1994.160
Baseline IPC (kNm)	350.948	685.019	1058.651	1434.220	396.018	753.735	1144.278	1630.281
CEMPC-IPC (kNm)	341.486	632.300	926.773	1264.573	396.053	728.194	1098.685	1514.710
Standard deviation of rotating low-speed shaft $(\sigma_{M_{lss}})$								
Baseline (kNm)	1100.345	1278.814	1522.350	1799.263	1474.161	1676.542	1962.194	2310.552
Baseline IPC (kNm)	375.454	622.960	894.843	1176.211	483.679	816.804	1171.619	1546.930
CEMPC-IPC (kNm)	404.949	638.005	890.900	1200.994	501.051	806.703	1141.918	1518.826
Standard deviation of fixed yaw bearing yaw moment $(\sigma_{M_{yb}})$								
Baseline (kNm)	384.151	712.070	1052.017	1392.475	478.646	894.101	1317.172	1748.134
Baseline IPC (kNm)	343.325	607.805	887.502	1174.124	438.233	771.345	1121.147	1490.183
CEMPC-IPC (kNm)	359.330	606.845	875.353	1161.360	449.448	769.436	1109.004	1479.080
Cumulative pitch travel distance (β_{tot})								
Baseline (deg)	130.062	264.841	408.633	559.424	149.628	300.342	453.346	614.807
Baseline IPC (deg)	2014.433	2096.757	2240.568	2438.766	2460.793	2544.232	2678.088	2888.781
CEMPC-IPC (deg)	2131.821	2473.935	2983.453	3618.730	2598.891	3034.297	3596.848	4416.405

Abbreviations: CEMPC, convex EMPC; IPC, individual pitch control; OoP, out-of-plane.